Ultra-Small Damage Detection via EIT in Soft Nanocomposite Sensors

Andrea Goh[a], Ananya Prasad[a], Tyler N. Tallman[a]

[a] *Purdue University, West Lafayette, Indiana, 47907, United States*

Abstract

Electrical impedance tomography (EIT) has received much attention as a potential sensing modality in robotic, biomedical, human-interfacing, and even structural applications. To date, however, work in this area has focused on sensing relatively large artifacts via EIT—spatially large pressure distributions, sizable damages in composites, large cracks in conductive coatings, etc. This is important because it is often much more desirable to detect *early stage* damage before it grows. EIT tends to struggle with small damage detection because the method is predicated on the damage causing a measurable voltage change at the domain's boundary. Small damages cause only small boundary voltage perturbations, which can easily be masked by noise. Additionally, commonly used regularizers such as the Laplace operator tend to "smooth over" small damages further masking them. With these limitations in mind, this manuscript makes three contributions: First, a mixed regularization scheme is implemented in the EIT inverse problem. Prior work has shown that this regularizer excels at finding small, highly localized damage. Second, the effect of injection-measurement scheme is explored. And third, a novel EIT test fixture is used that overcomes many of the challenges associated with experimental EIT. Experimental validation is conducted on a representative piezoresistive nanocomposite sensor, carbon nanofiber (CNF)-modified polyurethane (PU), which can be envisioned as a distributed pressure sensor, an artificial or robotic skin, or a sensing coating applied to a structural component. Our results show that with appropriate regularization and injection-measurement schemes, EIT can indeed find very small defects that are on the order of 0.0027% of the sensor's area. These results represent an order-of-magnitude improvement over the current state of the art.

Keywords: damage sensing, electrical impedance tomography, inverse problems, nanocomposite

1. Introduction

Electrical impedance tomography (EIT) is a method of spatially mapping the electrical conductivity of a domain. Because electrical conductivity is often coupled with material condition (e.g., stress/strain, temperature, damage, moisture content, etc.), EIT has been widely explored as a sensing modality [1]. A few representative applications include pressure sensing in soft materials (often nanocomposites) [2–9], damage detection and localization in fiber-reinforced composites [10–15], biomedical implant monitoring [16], and, among other examples, moisture flow monitoring in construction materials [17, 18].

Despite the abundance of work in the area of damage detection via EIT, work to date has focused on detecting relatively large artifacts. That is, in the current literature, it is often the case that EIT is detecting damage that is fairly obvious to the naked eye, thereby effectively eliminating the need for any kind of sensing technology. This is important because, especially with regard to damage detection, we typically want to find the damage when it is small and before it has a chance to grow catastrophically large.

In existent literature on small damage detection, Nonn et al. [19] used EIT to find through holes as small as 0.03% of the domain's surface area in carbon fiber composites. Gallo and Thostenson [20] found through holes measuring 1.22% of the domain's surface area in carbon nanotube (CNT)-modified glass fiber/epoxy laminates. Haingartner et al. [21] studied the effect of different injection patterns to find damage as small as 0.03% of the domain's surface area in carbon fiber composites. And as a final example, Tallman et al. [22] used EIT to find through-hole damage measuring 0.035% of the domain.

In these examples, although the small damage was *arguably* detected, good localization was generally not achieved (i.e., the EIT-predicted conductivity changes are much larger in size than the damage, do not collocate well with the damage, etc.), which is likely a consequence of the regularization used. Nonn et al. [19] and Haingartner et al. [21] used the diagonal of the sensitivity matrix (as part of the NOSER algorithm), Gallo and Thostenson [20] used the identity matrix, and Tallman et al. [22] used the discrete Laplace operator. None of these regularizers are adept at finding small, highly localized features as is the case for small damages. Alternatively, Fan and colleagues [23–25] used more sophisticated ℓ_1-norm regularization formulations along with machine learning to find and much better localize small damage in carbon fiber composites, achieving defect detection on the order of 0.07% of the domain size. The work of Fan and colleagues emphasizes how important appropriate regularization—in this case, a sparsity-promoting formulation—is to effectively finding small features via EIT.

These examples highlight two important points: First, even if EIT can detect small damages, image quality and localization are highly dependent on implementing regularization that is well suited to small artifacts. For example, regularization using the ℓ_1-norm promotes a sparse solution, which is much better suited to small damage detection. That is, physically, we expect the EIT solution to have zero conductivity change everywhere *except* where there is damage. Sparsity-promoting regularization via the ℓ_1-norm aligns with this expectation much better than regularization via the ℓ_2-norm, which is most commonly used in the state of the art. And second, even though 0.03% of the domain size sounds like a very small defect, this still corresponds to a 10 mm hole in a 500 mm $\times$ 500 mm plate. A 10 mm hole can be found just by visual inspection (i.e., something as sophisticated as EIT is not necessary to find this damage). Thus, the limit of detectability by EIT needs to be driven even lower for this technology to have merit as a sensing and inspection tool.

In light of the preceding discussion, this manuscript seeks to advance the state of the art by making **three novel contributions**: First, we implement a mixed regularization formulation into the EIT inverse problem to find small damages. The mixed regularization, originally developed by Homa and colleagues for damage detection in structural composites [26, 27], excels at finding small and highly localized features like damage while simultaneously suppressing non-relevant indications due to noise. This regularization term is also incorporated into an ℓ_1 error norm for improved robustness to outlier data in EIT measurements. Second, we explore the effect of different injection-measurement schemes on small damage detection. EIT is predicated on artifacts causing changes in boundary voltage greater than the noise threshold, so detecting small damages (which cause only very small changes in boundary voltages) is very much dependent on the injection-measurement scheme. And third, we demonstrate a novel experimental EIT fixture that eliminates the need for cumbersome and often unreliable electroding methods such as conductive adhesives and tape.

Two experimental validation cases are conducted: 1) small hole detection and 2) small cut detection in carbon nanofiber (CNF)-modified polyurethane (PU). CNF/PU is selected as a representative self-sensing material that can be easily produced as a thin sheet. This material can be envisioned as being a soft distributed pressure sensor, an artificial skin, or a sensing layer applied to a structural component. Our results show that EIT can indeed detect very small defects, on the order of 0.0027% of the domain size, which is an order of magnitude smaller than comparable

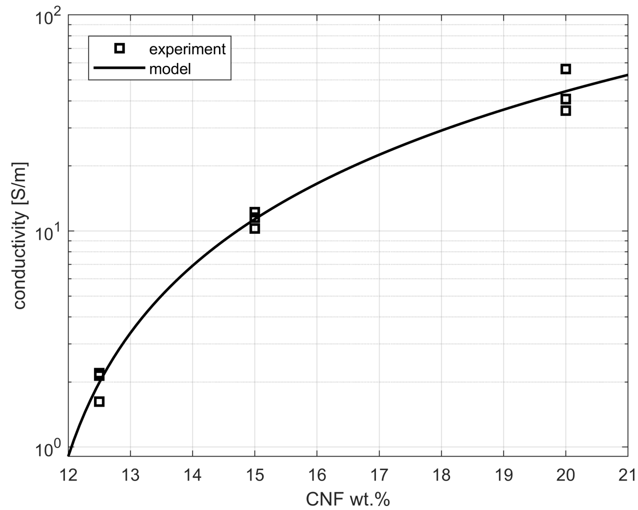

Figure 1: CNF/PU conductivity versus CNF wt.%. The material exhibits percolation-like behavior typical of nanocomposites.

studies in the current state of the art.

2. CNF/PU Manufacturing and Conductivity

CNF (Pyrograf III-PR-24-XT-HHT from Applied Sciences)-modified PU was used as a representative piezoresistive material in this research because it is low cost and easily produced in our laboratory. CNFs are comprised of stacked cone-like carbon structures with aspect ratios between 250 and 2000 [28]. CNFs cost less than carbon nanotubes (CNTs) and possess similar mechanical (elastic modulus of 240 GPa and tensile strength of 2.92 GPa [29]) and electrical (conductivity of 10^5 S/m [30]) properties.

CNFs were dispersed in a two-part PU (ReoFlex 20 from Smooth-On, Inc.) via the following procedure: First, appropriate amounts of CNFs were weighed out and mixed by hand into the PU. Half of the total desired CNF weight fraction was dispersed in each part of the two-part PU. Second, each CNF + PU part was mixed individually for five minutes in a Thinky AR-100 planetary centrifugal mixer. Third, both mixtures were degassed in a vacuum chamber at room temperature for five minutes. Fourth, the two parts were combined and roughly mixed by hand. Fifth, the combined mixture was then mixed in the planetary centrifuge for 20 seconds and degassed in a vacuum chamber at room temperature for five minutes. Sixth, the combined mixture was evenly spread into a mold measuring 150 mm $\times$ 120 mm $\times$ 1 mm. Seventh, the spread mixture was allowed to cure at room temperature for 24 hours. And lastly, the specimen was removed from the mold and cured for an additional 8 hours at 80 °C.

Several specimens were produced at 12.5, 15, and 20 wt.% CNFs by following this process. The electrical conductivity of the CNF/PU as a function of CNF weight fraction is shown in Figure 1. These data were also fit to an electrical percolation curve of the form $\sigma = a\,(\text{wt.\%} - b)^c$, where σ is the CNF/PU volume conductivity and a, b, and c are curve-fitting parameters. A CNF weight fraction of 14% was selected as a tradeoff between conductivity and processability.

3. Electrical Impedance Tomography

EIT has two parts: the forward problem and the inverse problem. The forward problem predicts the electrode voltages for a given conductivity distribution, whereas the inverse problem predicts the conductivity distribution for a given set of electrode voltages. EIT ultimately seeks to find a conductivity distribution that, when supplied to the forward problem, minimizes the difference between model-predicted and experimentally measured electrode voltages.

3.1. Forward Problem

The forward problem is governed by Laplace's equation for steady-state diffusion in the absence of internal current sources. This is shown in equation (1).

$$\nabla \cdot \sigma \nabla \phi = 0 \tag{1}$$

Above, σ is the conductivity, and ϕ is the electric potential in the domain. Equation (1) is subject to the complete electrode model (CEM) boundary conditions [31] as shown in equations (2)–(4).

$$\phi + z_l \sigma \nabla \phi \cdot n = V_l \tag{2}$$

$$\sum_{l=1}^{L} \int_{E_l} \sigma \nabla \phi \cdot n \, \mathrm{d}E_l = 0 \tag{3}$$

$$\sigma \nabla \phi \cdot n = 0 \quad \text{on} \quad x \in \partial\Omega \backslash \bigcup_{l=1}^{L} E_l \tag{4}$$

L is the total number of electrodes, z_l is the contact impedance between the domain and the lth electrode, n is an outward-pointing normal vector, V_l is the voltage on the lth electrode, E_l is the size of the lth electrode, and $\partial\Omega$ is the boundary of the domain. Equations (2)–(4) respectively enforce a voltage drop between the domain and the electrodes due to contact impedance, conservation of charge, and that current only passes through electrodes.

Interested readers are directed to other references for the finite element-discretized forms of these equations [1, 32]. A two-dimensional mesh of linear triangular elements was used in this work, and the surface-mounted electrodes were simulated by cutting out the electrode area and applying the current on the edges of the cut out area as described in [33].

3.2. Inverse Problem

We used time-difference imaging in this work, which means that EIT measurements are collected before damage and again after damage. EIT then seeks to find the *change* in conductivity between states. Let y be the voltage difference vector, where V_m is a vector of inter-electrode voltage differences measured at times t_1 and t_2.

$$y = V_m(t_2) - V_m(t_1) \tag{5}$$

This vector can also be defined using the forward model as shown next in equation (6).

$$W = F(\sigma + x) - F(\sigma) \tag{6}$$

In equation (6), $F(\sigma)$ is a vector of forward model-predicted inter-electrode voltages, and x is the conductivity change that we seek. $F(\sigma + x)$ can be linearized by a Taylor series expansion as $F(\sigma + x) \approx F(\sigma) + \frac{\partial F(\sigma)}{\partial \sigma} x$. The sensitivity matrix is then defined as $J = \frac{\partial F(\sigma)}{\partial \sigma}$.

Using this linearization, W can be rewritten as $W \approx Jx$. The EIT inverse problem is solved by treating it as an optimization problem, wherein we seek an x that minimizes the difference between the linearized form of W and y as shown in (7).

$$x^* = \min_{x \leq 0} |Jx - y|_1^1 + \alpha \, ||Rx||_2^2 \tag{7}$$

Above, x^* is the conductivity change satisfying the minimization, α is a hyperparameter dictating the amount of regularization, and R is the regularization term. A negativity constraint is also enforced because damage is physically expected to cause a conductivity loss.

The prevailing approach in the state of the art is to minimize the ℓ_2-norm of the error term, $Jx - y$, because this is easily done via standard tools like 'lsqlin' in MATLAB. However, squaring the error term makes EIT very susceptible to outlier data. We therefore instead opt to minimize the ℓ_1-norm of the error. This has the benefit of being much more robust to outlier data but has the drawback of being harder to solve due to the non-differentiability of this norm. Fortunately, the primal-dual interior point method (PDIPM) is a well-established method of solving equation (7).

The PDIPM solves equation (7) through the use of a dual optimization problem that is solved simultaneously [34–36]. Solving for x as shown in equation (7) is the primal problem, and solving for z as shown in equation (8) is the dual problem.

$$z^* = \max_{z} \begin{cases} z^T \left(Jx - y \right) + \alpha \, ||Rx||_2^2 & : \; |z_i| \leq 1 \\ J^T z + \alpha R^T R x = 0 \end{cases} \tag{8}$$

x and z are calculated iteratively as $x^{n+1} = x^n + \delta x$ and $z^{n+1} = z^n + \min\left(1, \, \kappa\right) \delta z$. κ is selected such that $\kappa = \sup\left(\kappa : \; |z_i^n + \kappa \delta z_i| \leq 1\right)$ for the $n+1$ iteration by solving the system of equations shown in equation (9). $\left(Jx - y\right)_i$ is the ith value of the error vector, z_i is the ith value of the dual vector, and β is a small scalar value.

$$\begin{bmatrix} 2\alpha R^T R & J^T \\ GJ & -E \end{bmatrix} \begin{bmatrix} \delta x \\ \delta z \end{bmatrix} = - \begin{bmatrix} J^T z + 2\alpha R^T R x \\ \left(Jx - y\right) - Ez \end{bmatrix} \tag{9}$$

$$E = \mathrm{diag}\left(\left(\left(Jx - y\right)_i^2 + \beta \right)^{\frac{1}{2}} \right) \tag{10}$$

$$G = \mathrm{diag}\left(1 - \frac{z_i \left(Jx - y\right)}{\left(\left(Jx - y\right)_i^2 + \beta \right)^{\frac{1}{2}}} \right) \tag{11}$$

3.3. Mixed Regularization

The detection of ultra-small damage is greatly aided by the use of the mixed prior for regularizing the EIT inverse problem. The mixed prior was originally developed by Homa and colleagues [26, 27] and is predicated on combining two regularizers: a smoothness prior and a focal prior as $R = L + \Lambda$. The smoothness prior, L, is the discretized form of the discrete Laplace operator, $\nabla^2 x$, and promotes spatially smooth solutions. This type of regularization is very commonly used by the EIT materials-imaging community. It has the benefit of being easy to implement and is well suited for imaging smoothly varying conductivity distributions such as those arising from strains [37], but it also has a tendency to "smooth over" small changes (e.g., due to small damages), making them indistinguishable from noise-induced artifacts.

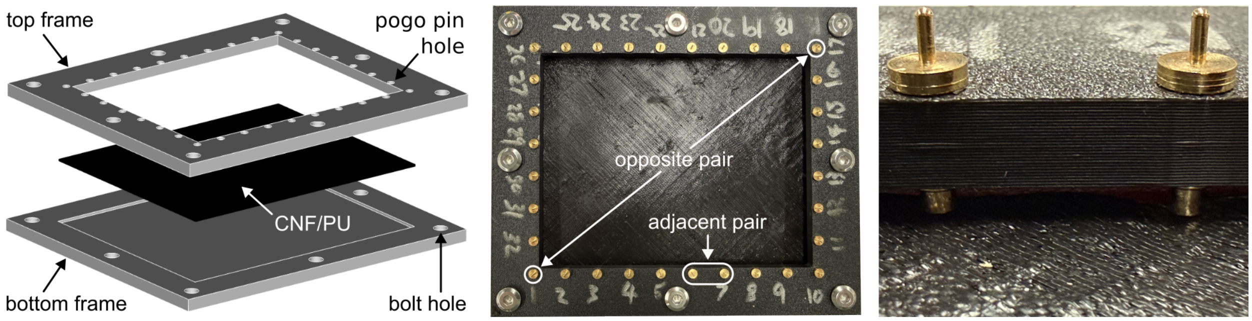

Figure 2: Left: CAD drawing of EIT fixture assembly. Middle: Top-down view of the fixture with electrodes numbered and a CNF/PU specimen inserted. Adjacent and opposite electrode pairs are also highlighted. Right: A close up view of the pogo pins showing contact with the surface of the CNF/PU.

The focal prior, Λ, ensures that conductivity changes only occur corresponding to statistically significant variations in the measurement data. This term is therefore excellent at suppressing non-relevant changes that arise from measurement noise, but it has the drawback of not requiring that conductivity changes be connected in a way that is physical (i.e., it can give rise to "jagged" conductivity distributions). Combined, the smoothness + focal terms ensure that conductivity changes only arise from significant variations in the measurement data *and* are smoothly grouped together, which is a reasonable expectation for small and highly localized damages. Deriving the focal term exceeds the scope of this manuscript, but interested readers are directed to the works of Homa and colleagues [26, 27] for details.

4. Experimental Methods

4.1. EIT Measurement Fixture

Robust electrode connections are a challenging part of experimental EIT. A combination of conductive silver-based adhesive and copper tape is often used when applying EIT to materials, but this process is slow, messy, and prone to failure (e.g., the adhesive breaks, the tape falls off, etc.). Therefore, we developed an EIT test fixture. This fixture, shown in Figure 2, is essentially a two-part frame that sandwiches the 150 mm $\times$ 120 mm $\times$ 1 mm CNF/PU sheet between a top frame and a bottom frame. The frames were printed using a Bambu Lab P1S printer. Electrical contact is made with pogo pins inserted into the top part of the frame. Pogo pins are spring-loaded pins that ensure a constant pressure is applied between the pin and the CNF/PU when the two parts of the frame are bolted together. This particular fixture had a total of 32 electrodes. Based on our research group's extensive experience with EIT, the EIT fixture used in this work provided much more stable measurements than silver adhesive + copper tape electrodes. It is also quick and easy to insert new sheets for testing.

4.2. Injection and Measurement Procedures

In order for EIT to have any chance of working, damage-induced changes in electrode voltages must exceed the noise in the measurements. Small damages result in only minute changes in boundary voltage. Thus, our intent in studying the effect of different injection-measurement schemes was to see if different schemes are more or less sensitive to small damages. A total of four injection-measurement schemes were tested. To clarify, an injection-measurement scheme refers to electrodes between which current is injected (i.e., injected and grounded) and between which voltage is measured. For this, we considered all permutations of adjacent and opposite electrode

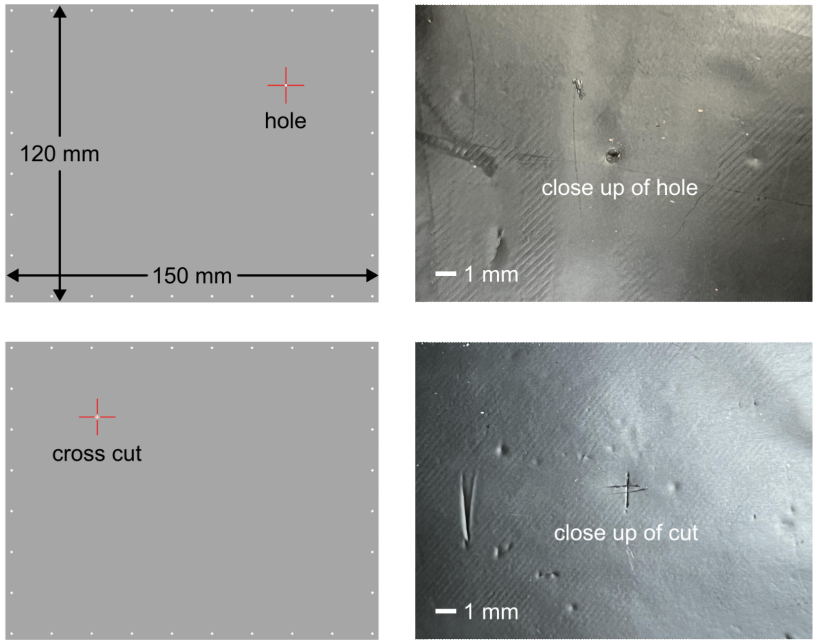

Figure 3: Left column: Placement of the hole and cut damage in two different CNF/PU sheets. Note the red lines indicate the center of the damage, and the white indicates the actual damage size. White holes near the boundary are electrodes. Right column: Close up images of the hole and cut damages.

pairs. Illustrated in the middle of Figure 2, adjacent electrode pairs are directly neighboring (e.g., electrodes 1 and 2, 2 and 3, 3 and 4, etc. are adjacent pairs). Opposite electrode pairs are on opposite sides of the domain such that the difference between the electrode numbers is 16 (e.g., electrodes 1 and 17, 2 and 18, 3 and 19, etc. are opposite pairs). The four permutations of these pairs are as follows: 1) adjacent injections and adjacent measurements, 2) adjacent injections and opposite measurements, 3) opposite injections and adjacent measurements, and 4) opposite injections and opposite measurements. Injections continue until current has been injected into every single electrode. For a particular injection, the voltages are measured between every electrode pair.

Electrical currents of 0.5 mA were injected using a Keithley 6221 current supply, and voltages were measured using National Instruments PXIe-6368 data acquisition cards. Voltage measurements were taken with respect to ground such that inter-electrode differences could be calculated offline.

4.3. Damage

Two different CNF/PU specimen were tested. One was subjected to through-hole damage, and the other was subjected to two small cuts arranged as a cross. Shown in Figure 3, the hole was induced by manually twisting a 1/32" (0.79 mm) drill bit into the surface of the CNF/PU. The cross cut was induced using an X-Acto knife.

5. Results and Discussion

Hole detection results are shown in Figure 4, and cut detection results are shown in Figure 5. Examining these results, we can make several noteworthy observations. First, generally speaking, EIT with appropriate regularization can indeed detect and localize these small damages. The

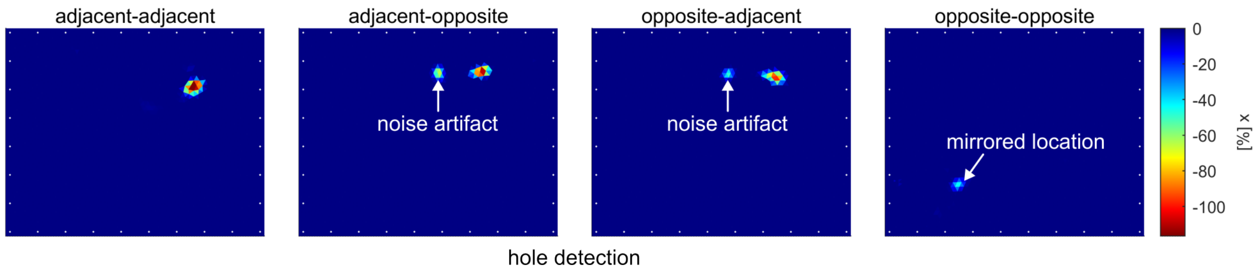

Figure 4: Small hole detection via EIT using adjacent-adjacent, adjacent-opposite, opposite-adjacent, and opposite-opposite injection-measurement schemes. Of the schemes tested, adjacent-adjacent performs the best. It detects and localizes the small hole without noise artifacts and without mirroring effects.

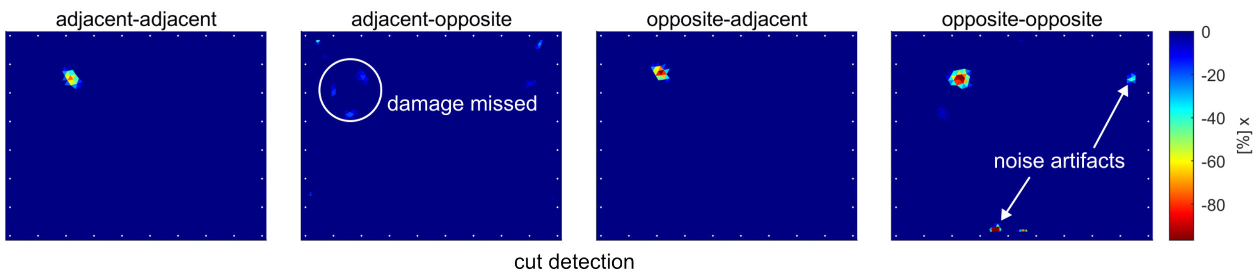

Figure 5: Small cut detection via EIT using adjacent-adjacent, adjacent-opposite, opposite-adjacent, and opposite-opposite injection-measurement schemes. Both the adjacent-adjacent and opposite-adjacent schemes performed well for this damage case. Except for some small non-relevant indications, the opposite-opposite scheme also performed well, but the adjacent-opposite scheme missed the cut entirely.

hole is approximately 0.0027% of the CNF/PU sheet's surface area, which represents an order-of-magnitude improvement over the current state of the art (i.e., existent literature has found holes on the order of 0.03% of the domain's area). Further, compared to other works in this area, the mixed prior achieves much better localization; conductivity changes are tightly grouped in the immediate vicinity of the damage.

Second, even though EIT was generally able to detect the small damages, not all injection-measurement schemes performed equally. The adjacent-adjacent scheme performed the best between the two damage cases; it adeptly detected and localized both the hole and the cut with no non-relevant indications. The opposite-adjacent scheme performed the second best. This scheme clearly found both damages, but it also had a non-relevant indication for the hole detection case in Figure 4. Of the remaining two injection-measurement schemes, adjacent-opposite and opposite-opposite, we do not feel that one definitively performed better than the other. The adjacent-opposite scheme clearly found the hole (albeit with non-relevant indication), but it missed the cut entirely. The opposite-opposite scheme clearly found the cut (again with some non-relevant indications), but it *mirrored* the hole damage. Reported elsewhere [38, 39], mirroring (or ghosting) is a consequence of the total symmetry in both the injections and measurements, which renders EIT as unable to discern on which side of a symmetry plane the artifact exists.

Third, even though the mixed prior is excellent at suppressing non-relevant indications due to noise, a few are observed in these results. This is likely a consequence of the fact that, owing to the extremely small size of the damage, the voltage change at the boundary is extremely small and at times not entirely distinguishable from noise.

Fourth, it is worth considering the magnitude of EIT-predicted conductivity change. That is, for the case of a hole, we physically expect a 100% loss of conductivity. EIT regularized by the mixed prior over-predicts the conductivity loss slightly, but the predicted change is nonetheless

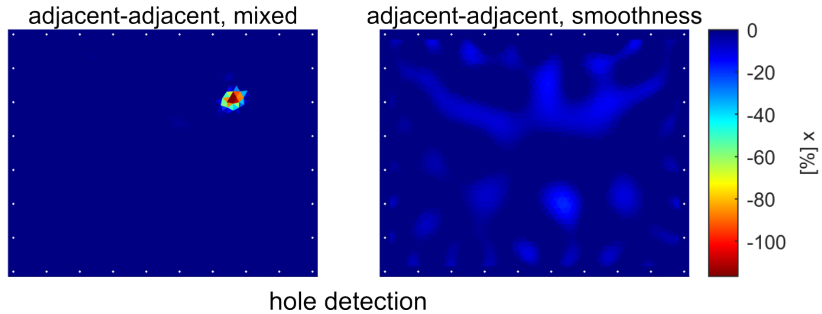

Figure 6: A comparison of the mixed and smoothness-only regularizations for hole detection using the adjacent-adjacent injection-measurement scheme. The smoothness-only approach misses the small hole entirely.

close to 100%. For the case of a cut, EIT predicts a conductivity change of less than 100%. This is perhaps not unexpected considering that the cut faces are in contact with each other (i.e., some current can still pass between the faces where they are in contact).

Lastly, it is informative to compare the results obtained by using the mixed prior for regularization to those obtained by using just the smoothness prior (i.e., the Laplace operator). This comparison is shown in Figure 6 for the case of hole detection using the adjacent-adjacent injection-measurement scheme. Only this particular injection-measurement scheme and damage case are considered for this comparison because it is representative of all the results. Whereas the mixed formulation clearly finds the hole, using only the smoothness prior for regularization entirely misses the damage. One could perhaps make an argument that there is a faint, blobular conductivity change in the area of the hole (an argument that is made regrettably often in EIT literature), but we assert that this is only wishful thinking—the smoothness-only regularization fails to find the small hole. This underscores the importance of judicious regularization selection for EIT. The regularization term *must* be selected to match the expectations of the artifact being imaged.

6. Summary and Conclusions

In summary, this work has explored the effect of advanced regularization techniques and injection-measurement schemes for small damage detection via EIT. This work was motivated by the potential of EIT as a sensing modality across diverse application spaces, the importance of accurate early-stage damage detection, and the inadequacy of existent EIT formulations to find very early stage damage. Procedurally, soft CNF-modified PU sheets were produced as representative distributed sensors. CNF/PU sheets were then inserted into a custom-made EIT fixture that uses a two-part frame with integrated pogo pin arrays to ensure robust and stable electrical contact with the specimen. Two damage cases were considered in this manuscript: a small through hole and a small cut. Using the mixed prior, EIT was able to detect and localize both damages. Of the schemes tested, the adjacent-adjacent injection-measurement scheme qualitatively performed the best.

Based on the results and discussion presented in this manuscript, we can draw the following conclusions about small damage detection via EIT.

- Conclusion 1) EIT can indeed detect small damages.
  Our results show that EIT can find damages as small as 0.0027% of the domain's area, which is a significant improvement over existent results published in the current state of the art. Further, both small hole and small cut damages were successfully found via EIT.

- Conclusion 2) Small damage detection is highly dependent on appropriate regularization.
  As demonstrated in Figure 6, the effectiveness of EIT for small damage detection depends

heavily on regularization. To wit, not all regularization terms are suited for all artifacts. Herein, the mixed prior worked well for small, highly localized artifacts, but other works have shown that it does not work well for imaging distributed features (e.g., long cracks [40]). It is incumbent on the EIT practitioner to select regularization that is suited to their imaging needs.

- Conclusion 3) Injection-measurement scheme also impacts small damage detection.
  All of the tested injection-measurement schemes were able to find at least one of the damage cases. However, all of the schemes, other than the adjacent-adjacent scheme, produced noticeable non-relevant indications, mirroring effects, or missed one damage case entirely. These differences are likely a consequence of the signal-to-noise ratio (SNR) of each scheme for each damage case. That is, for the particular damage cases tested in this manuscript, adjacent-adjacent happened to do best. More generally, however, it is advisable to test numerous injection-measurement schemes when calibrating to a new damage type, location, etc.

- Conclusion 4) Small damage detection is greatly aided by test fixtures capable of providing stable measurements.
  Speaking of SNR in the previous point, based on the authors' extensive experience using EIT for material imaging, it is our opinion that the results obtained in this manuscript were *greatly* facilitated by the high-quality measurements taken using the EIT fixture. As mentioned previously in section 4.1, much materials imaging via EIT uses a combination of conductive silver-based epoxy adhesives and copper tape for electroding. Electrodes made of these materials are prone to breaking, decaying over time, falling or peeling off, or giving otherwise unstable measurements (which requires reattachment of the electrode). The test fixture used in this work, on the other hand, gave stable and consistent measurements, which greatly improved the SNR of the data. Further, it was low cost and easy to make. Similar fixtures are recommended in future work.

Acknowledgments

This work was supported by Samsung Electronics Co., Ltd. (TCS Project Code: IO241217-11501-01).

Competing Interests

The authors declare that they have no known competing financial interests or personal relationships that could have appeared to influence the work reported in this paper.

References

[1] T. N. Tallman, D. J. Smyl, Structural health and condition monitoring via electrical impedance tomography in self-sensing materials: a review, Smart Materials and Structures 29 (12) (2020) 123001.

[2] R. Ellingham, C. Pretty, L. Holder-Pearson, K. Aw, T. Giffney, An electrical impedance tomography based artificial soft skin pressure sensor: Characterisation and force modelling, Sensors and Actuators A: Physical 373 (2024) 115427.

[3] L. Sun, S. Jiang, Y. Xiao, W. Zhang, Realization of flexible pressure sensor based on conductive polymer composite via using electrical impedance tomography, Smart Materials and Structures 29 (5) (2020) 055004.

[4] H. Chen, K. Langlois, J. Brancart, E. Roels, T. Verstraten, B. Vanderborght, A novel physical human–robot interface with pressure distribution measurement based on electrical impedance tomography, IEEE Sensors Journal 23 (18) (2023) 21914–21923.

[5] R. Ellingham, L. Holder-Pearson, C. Pretty, T. Giffney, A portable electrical impedance tomography based pressure mapping sensor and force localisation validation system, HardwareX 21 (2025) e00628.

[6] H. Chen, X. Yang, P. Wang, J. Geng, G. Ma, X. Wang, A large-area flexible tactile sensor for multi-touch and force detection using electrical impedance tomography, IEEE Sensors Journal 22 (7) (2022) 7119–7129.

[7] T. Tallman, S. Gungor, K. Wang, Tactile imaging and distributed strain sensing in highly flexible carbon nanofiber/polyurethane nanocomposites, Carbon 95 (2015) 485–493.

[8] E. Smela, Electrical Impedance Tomography for Tactile Imaging: A Primer for Experimentalists, IOP Publishing, 2024.

[9] S. Russo, S. Nefti-Meziani, N. Carbonaro, A. Tognetti, A quantitative evaluation of drive pattern selection for optimizing eit-based stretchable sensors, Sensors 17 (9) (2017) 1999.

[10] X. Cheng, J. Liu, K. Zheng, Z. Wu, L. Shi, X. Hu, Monitoring of damage evolution in carbon fiber reinforced polymer composites by electrical impedance tomography, NDT & E International 148 (2024) 103239.

[11] F. Hao, S. Wang, F. Xing, M. Li, T. Li, Y. Gu, W. Zhang, J. Zhang, Carbon-nanotube-film-based electrical impedance tomography for structural damage detection of carbon-fiber-reinforced composites, ACS Applied Nano Materials 4 (5) (2021) 5590–5597.

[12] L. W. Escalona Galvis, P. Diaz-Montiel, S. Venkataraman, Optimal electrode selection for electrical resistance tomography in carbon fiber reinforced polymer composites, Materials 10 (2) (2017) 125.

[13] J. Cagáň, J. Pelant, M. Kyncl, M. Kadlec, L. Michalcová, Damage detection in carbon fiber–reinforced polymer composite via electrical resistance tomography with gaussian anisotropic regularization, Structural Health Monitoring 18 (5-6) (2019) 1698–1710.

[14] H. Rocha, C. Fernandes, N. Ferreira, U. Lafont, J. P. Nunes, Damage localization on cfrp composites by electrical impedance tomography, Materials Today Communications (2022) 104164.

[15] W. Lestari, B. Pinto, V. La Saponara, J. Yasui, K. J. Loh, Sensing uniaxial tensile damage in fiber-reinforced polymer composites using electrical resistance tomography, Smart Materials and Structures 25 (8) (2016) 085016.

[16] H. Ghaednia, C. E. Owens, R. Roberts, T. N. Tallman, A. J. Hart, K. M. Varadarajan, Interfacial load monitoring and failure detection in total joint replacements via piezoresistive bone cement and electrical impedance tomography, Smart Materials and Structures 29 (8) (2020) 085039.

[17] D. Smyl, M. Hallaji, A. Seppänen, M. Pour-Ghaz, Three-dimensional electrical impedance tomography to monitor unsaturated moisture ingress in cement-based materials, Transport in Porous Media 115 (2016) 101–124.

[18] G. Kłosowski, A. Hoła, T. Rymarczyk, Ł. Skowron, T. Wołowiec, M. Kowalski, The concept of using lstm to detect moisture in brick walls by means of electrical impedance tomography, Energies 14 (22) (2021) 7617.

[19] S. Nonn, M. Schagerl, Y. Zhao, S. Gschossmann, C. Kralovec, Application of electrical impedance tomography to an anisotropic carbon fiber-reinforced polymer composite laminate for damage localization, Composites Science and Technology 160 (2018) 231–236.

[20] G. J. Gallo, E. T. Thostenson, Spatial damage detection in electrically anisotropic fiber-reinforced composites using carbon nanotube networks, Composite Structures 141 (2016) 14–23.

[21] M. Haingartner, S. Gschoßmann, M. Cichocki, M. Schagerl, Improved current injection pattern for the detection of delaminations in carbon fiber reinforced polymer plates using electrical impedance tomography, Structural Health Monitoring 20 (5) (2021) 2747–2757.

[22] T. N. Tallman, S. Gungor, K. Wang, C. E. Bakis, Damage detection via electrical impedance tomography in glass fiber/epoxy laminates with carbon black filler, Structural Health Monitoring 14 (1) (2015) 100–109.

[23] Y. Cheng, W. Fan, R-unet deep learning-based damage detection of cfrp with electrical impedance tomography, IEEE Transactions on Instrumentation and Measurement 71 (2022) 1–8.

[24] A. W. Fan, B. Y. Cheng, Sorted l 1 regularization method for damage detection based on electrical impedance tomography, Review of Scientific Instruments 92 (12) (2021) 124701.

[25] Q. Xue, C. Chen, W. Fan, Damage detection of cfrp laminates based on adamax-inn model for eit, Measurement Science and Technology 35 (2) (2023) 025405.

[26] L. Homa, M. Sannamani, A. J. Thomas, T. N. Tallman, J. Wertz, Enhanced damage imaging in three-dimensional composite structures via electrical impedance tomography with mixed and level set regularization, NDT & E International 137 (2023) 102830.

[27] T. N. Tallman, L. Homa, M. Flores, J. Wertz, Damage mapping via electrical impedance tomography in complex am shapes using mixed smoothness and bayesian regularization, Computer Methods in Applied Mechanics and Engineering 414 (2023) 116185.

[28] M. H. Al-Saleh, U. Sundararaj, Review of the mechanical properties of carbon nanofiber/polymer composites, Composites Part A: Applied Science and Manufacturing 42 (12) (2011) 2126–2142.

[29] G. G. Tibbetts, J. J. McHugh, Mechanical properties of vapor-grown carbon fiber composites with thermoplastic matrices, Journal of Materials Research 14 (7) (1999) 2871–2880.

[30] S. Bal, Experimental study of mechanical and electrical properties of carbon nanofiber/epoxy composites, Materials & Design (1980-2015) 31 (5) (2010) 2406–2413.

[31] E. Somersalo, M. Cheney, D. Isaacson, Existence and uniqueness for electrode models for electric current computed tomography, SIAM Journal on Applied Mathematics 52 (4) (1992) 1023–1040.

[32] A. Adler, D. Holder, Electrical impedance tomography: methods, history and applications, CRC Press, 2021.

[33] J. Jauhiainen, M. Pour-Ghaz, T. Valkonen, A. Seppänen, Nonplanar sensing skins for structural health monitoring based on electrical resistance tomography, Computer-Aided Civil and Infrastructure Engineering 36 (12) (2021) 1488–1507.

[34] T. Tallman, J. Hernandez, The effect of error and regularization norms on strain and damage identification via electrical impedance tomography in piezoresistive nanocomposites, NDT & E International 91 (2017) 156–163.

[35] Y. Mamatjan, A. Borsic, D. Gürsoy, A. Adler, An experimental clinical evaluation of eit imaging with ℓ_1 data and image norms, Physiological measurement 34 (9) (2013) 1027.

[36] A. Borsic, A. Adler, A primal–dual interior-point framework for using the l1 or l2 norm on the data and regularization terms of inverse problems, Inverse Problems 28 (9) (2012) 095011.

[37] H. Hassan, T. N. Tallman, Failure prediction in self-sensing nanocomposites via genetic algorithm-enabled piezoresistive inversion, Structural Health Monitoring 19 (3) (2020) 765–780.

[38] T. Sun, S. Tsuda, K.-P. Zauner, H. Morgan, On-chip electrical impedance tomography for imaging biological cells, Biosensors and Bioelectronics 25 (5) (2010) 1109–1115.

[39] A. Thomas, J. Kim, T. Tallman, C. Bakis, Damage detection in self-sensing composite tubes via electrical impedance tomography, Composites Part B: Engineering 177 (2019) 107276.

[40] T. N. Tallman, D. Smyl, L. Homa, J. Wertz, The effect of different regularization approaches on damage imaging via electrical impedance tomography, Journal of Nondestructive Evaluation 44 (2) (2025) 1–14.